Martensitic and Magnetic Transformation Behavior of $Ni_{50}Mn_{38-x}In_{12}Fe_x$ Polycrystalline Alloys

WU Zhigang[1,2], REN Xiaobing[1], LIU Yinong[2]

(1. Multi-Disciplinary Materials Research Center, Frontier Institute of Science and Technology, Xi'an Jiaotong University, Xi'an 710049, China)

(2. School of Mechanical Engineering, The University of Western Australia, Crawley WA6009, Australia)

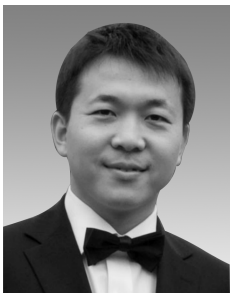

吴志刚

Abstract: The effect of Fe substitution for Mn on the martensitic and magnetic transformation behaviors of $Ni_{50}Mn_{38-x}In_{12}Fe_x$ (x = 0, 3, 4, 5, 6) polycrystalline alloys was investigated. A martensitic transformation from a B2 austenite to an orthorhombic martensite was observed with lower Fe contents ($x \leqslant 4$), while the transformation was completely suppressed with further increasing the Fe content ($x \geqslant 5$) of the alloys. Substitution of Fe for Mn at above 3% (x) introduced an fcc γ phase in the microstructure, the amount of which increased with increasing the Fe content. The γ phase influenced the composition of the matrix phase, as well as the e/a ratio, leading to a series change of the physical properties of the alloys. Firstly, the e/a ratio of the matrix phase decreased rapidly with increasing Fe content, resulting in the abrupt decrease of martensitic transformation temperature and enthalpy change. Secondly, Fe addition effectively increased the ferromagnetic ordering of the matrix phase, leading to the increase of the Curie transition temperatures and the magnetization of the alloys. The origin of the effect of Fe addition on changes in martensitic transformation and magnetic behaviour is discussed.

Key words: shape memory alloy; martensitic transformation; magnetic properties; intermetallics

CLC number: TG139$^+$.6 **Document code**: A **Article ID**: 1674 - 3962 (2013)02 - 0114 - 07

$Ni_{50}Mn_{38-x}In_{12}Fe_x$ 多晶合金的马氏体转变和磁转变特性

吴志刚[1,2]，任晓兵[1]，刘义农[2]

（1. 西安交通大学前沿科学与技术学院 多学科材料研究中心，陕西 西安 710049）

（2. 西澳大利亚大学机械工程学院，澳大利亚 克劳利 WA6009）

摘 要：详细研究了 $Ni_{50}Mn_{38-x}In_{12}Fe_x$（$x$ = 0，3，4，5，6）合金体系中 Fe 取代 Mn 对合金马氏体相变行为及磁学性能的影响。发现当 $x \leqslant 4$ 时，合金表现出由 B2 结构的奥氏体向正交结构的马氏体转变的相变行为，而当 $x \geqslant 5$ 时该相变被完全抑制。当 Fe 对 Mn 的取代超过 3% 时，合金的显微结构中出现 γ 相，并发现其数量随 Fe 含量的增加而增加。γ 相的形成改变了合金基体相成分，进而带来了基体相 e/a（每原子的电子浓度）值的变化，研究结果证明合金的一系列性能改变均与基体相 e/a 值的变化相关。第一，基体相 e/a（每原子的电子浓度）值随着 Fe 含量的增加而迅速减小，导致了合金马氏体相变温度、相变潜热及相变熵变的降低。第二，Fe 的引入有效地增强了合金基体相的铁磁性能，提高了合金的居里转变温度和合金的磁化强度。详细阐述了 Fe 的引入是合金马氏体相变及磁学性能变化的本质原因。

关键词：形状记忆合金；马氏体转变；磁特性；金属间化合物

1 Introduction

Ferromagnetic shape memory alloys Ni-Mn-Z (Z = In, Sn, Sb) have been widely investigated in the past few years as potential candidates for magnetic actuation. The large difference in magnetic state between the austenite and martensite produces high magnetic driving force for magnetic-field-induced martensitic transformation[1]. Substitution of Ni by Co is found to increase the ferromagnetic ordering of the austenite and to decrease that of the martensite, further increasing the magnetization difference of the martensitic transformation in Ni-Mn-Z (Z = Ga, Al, In, Sn, Sn, Sb) alloys[2-8]. As a result, > 1% strain has been realized in $Ni_{45}Co_5Mn_{36.7}In_{13.3}$ and $Ni_{43}Co_7Mn_{39}Sn_{11}$ alloys[2-3], demonstrating the promise of the alloys for actuation applications in smart systems.

Unfortunately, the intrinsic brittleness of these interme-

Received date: 2012 - 07 - 23

Foundation item: China Postdoctoral Science Foundation (2012M521764); National Natural Science Foundation of China (51201124)

Biography: Wu Zhigang, Born in 1982, Doctor

DOI: 10.7502/j.issn.1674 - 3962.2013.02.07

tallic compounds severely hinders their engineering application. To date, it has not been possible to process polycrystalline Ni-Mn-Z (Z = In, Sn, Sb) ferromagnetic shape memory alloys using conventional methods. It is known that the introduction of a ductile second phase is helpful in improving the ductility of the alloys, as initially discovered in Ni-Fe-Ga[9], Co-Ni-Ga[10] and Co-Ni-Al[11] alloys. Later, adding Fe and Co was found to form a ductile γ phase in Ni-Mn-Z (Z = Ga, In, Sn)[12-17], accordingly increasing the ductility of these alloys.

Apart from the improved ductility, addition of a fourth element to the ternary Ni-Mn-Z (Z = Ga, In, Sn, Sb) alloys alters the matrix composition, which causes a number of changes in the structure, thermal and magnetic properties. The effect of Fe substitution for Mn in Ni-Mn-Sn alloys has been found to decrease the martensitic transformation temperatures and increase the Curie transition temperatures of both the austenite and the martensite due to the alteration of matrix composition after forming the γ phase[18-20]. However, the origin of the Fe addition with respect to the changes in martensitic and magnetic properties was not thoroughly clarified and understood in these alloys. This study investigated the effects of Fe substitution for Mn on the physical properties changes in detail for a Ni-Mn-In alloy system. The addition of Fe alters the composition of the matrix phase due to the formation of γ phase, thus affecting the magnetic state and valence electron number of the alloys. Fe atoms occupying Mn site greatly affect the magnetic ordering of both the austenite and martensite of the alloys, giving rise to the Curie transition and magnetization variation. The relevant changes in the physical properties may have great impacts on their potential applications of these alloys. Therefore, the explanation of the effect of Fe addition provides useful guide for alloy design of Ni-Mn-In alloy system.

2 Experimental procedures

Bulk ingots of polycrystalline $Ni_{50}Mn_{38-x}In_{12}Fe_x$ (x = 0, 3, 4, 5, 6) alloys were prepared by means of arc melting in argon atmosphere using high purity x(Ni) = 99.99%, x(Mn) = 99.99%, x(In) = 99.99% and x(Fe) = 99.95%. The samples are referred to as Fe0, Fe3, Fe4, Fe5 and Fe6, based on the atomic percentage of Fe addition in the alloys. The button shaped ingots were heated at 1 173 K in vacuum for homogenization followed by furnace cooling to room temperature. Transformation behaviour of the alloys was studied by means of differential scanning calorimetry (DSC) using a TA Q10 DSC instrument with a cooling/heating rate of 10 K/min. Phase identification and crystal structures were determined by means of X-ray powder diffraction using a Siemens D5000 instrument with Cu-Kα radiation and transmission electron microscopy (TEM) using a Jeol 2100 instrument. Microstructures of the samples were studied with TEM and scanning electron microscopy (SEM) using a Zeiss 1555 instrument. The compositions were determined by means of X-ray energy dispersive spectrometry (EDS) equipped on SEM. Magnetic properties were studied using a superconducting quantum interference device magnetometer (SQUID).

3 Results and discussion

3.1 Microstructure and alloy composition

Figure 1 shows back-scattered electron (BSE) micrographs of the microstructures of the $Ni_{50}Mn_{38-x}In_{12}Fe_x$ (x = 0, 3, 4, 5, 6) alloys after homogenization treatment. The BSE microstructures of the alloys were examined without etching. The Fe0 and Fe3 samples (micrograph a and b) showed uniform single phase structure, without sign of a second phase. The black spots are solidification shrinkage pores formed during ingot casting. The Fe4, Fe5 and Fe6 samples showed a continuous matrix in light contrast and dispersed γ phase particles in dark contrast. The volume fraction of the γ phase increased with increasing Fe addition. The alloy Fe6 showed distinctive texture of the γ phase compared to Fe4 and Fe5, with straight and elongated γ phase grains.

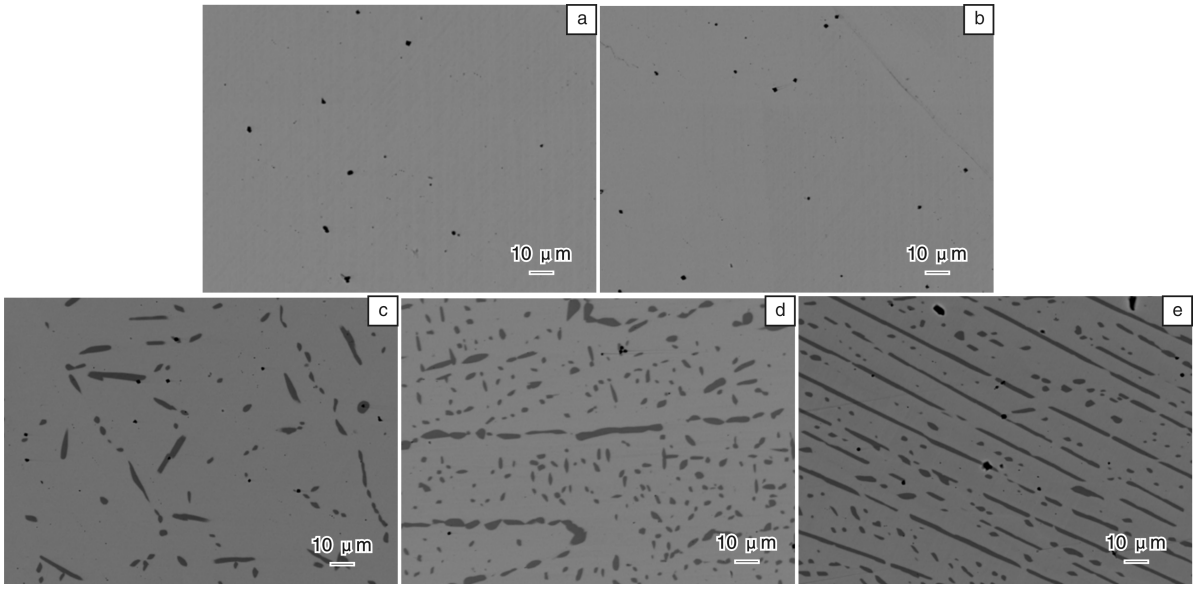

Fig. 1　Back-scattered electron images of the $Ni_{50}Mn_{38-x}In_{12}Fe_x$ alloys: (a) Fe0, (b) Fe3, (c) Fe4, (d) Fe5, and (e) Fe6 alloys

Table 1 shows compositions of the phases in the samples as determined by quantitative EDS analysis. It is seen that the matrix phase of the Fe-doped alloys contained about 49% (x) Ni. The content of Mn decreased continuously from

37.8% to 32.5% with increasing Fe addition from 2.9% to 3.8% in the matrix. The content of In was also found to increase from 12.8% to 14.8%. The γ phase is effectively a Ni-Mn-Fe alloy containing a small amount of In (~1.1% (x)). The volume fraction of the γ phase is determined by image analysis from the SEM micrographs using Image J. The increase of In content in the matrix phase is apparently related to the increase of the fraction of γ phase, which contains very little In. The valence electron concentrations per atom (e/a ratio) of the matrix phase was calculated using the compositions obtained from EDS analysis from the sum of s, p and d electrons for Mn (7), Ni (10), Fe (8) and In (3). It is obvious that the e/a ratio decreases with increasing In and decreasing Mn contents of the alloys.

Table 1 Composition, e/a ratio and γ proportion of $Ni_{50}Mn_{38-x}In_{12}Fe_x$ (x=0, 3, 4, 5, 6) alloys.

	Matrix/% (x)					The γ phase/% (x)				
	Ni	Mn	In	Fe	e/a ratio	Ni	Mn	In	Fe	Y/%
x=0	49.4	37.8	12.8	–	7.970	–	–	–	–	–
x=3	48.6	35.3	13.2	2.9	7.962	–	–	–	–	–
x=4	49.1	34.0	13.7	3.2	7.958	54.5	31.1	1.1	13.3	6.8
x=5	49.1	33.0	14.4	3.5	7.936	54.0	30.9	1.1	14.0	11.5
x=6	48.9	32.5	14.8	3.8	7.913	52.5	30.2	1.1	16.2	14.0

With increasing Fe addition, both Fe and In contents in the matrix phase increased, and the Mn content decreased. The e/a ratio of the alloy decreased continuously with increasing Fe addition in the alloys. The decrease of the e/a ratio is obviously related to the composition change in the matrix phase caused by the formation of the γ phase. More specifically, the decrease of Mn (7 valence electrons) and increase of In (3 valence electrons) contents are the main reasons for the decrease of the e/a ratio, though Fe (8 valence electrons) content slightly increased as well in the matrix phase.

3.2 Martensitic transformation behaviour

Figure 2 presents DSC curves of the $Ni_{50}Mn_{38-x}In_{12}Fe_x$ alloys. It is seen that the martensitic transformation behaviour evolved progressively with increasing Fe addition in these alloys. The martensitic transformation is clearly observed for Fe0, Fe3 and Fe4 alloys, and the transformation temperatures decreased with increasing Fe addition in these alloys. The T_M temperatures were determined to be 440, 350 and 310 K for Fe0, Fe3, and Fe4 alloys, respectively. However, no transformation was detected in Fe5 and Fe6 alloys.

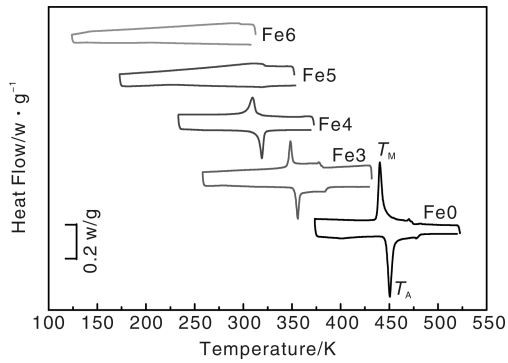

Fig. 2 DSC measurements of martensitic transformation behaviour of the $Ni_{50}Mn_{38-x}In_{12}Fe_x$ alloys

Figure 3 shows the effect of e/a ratio on transformation temperature T_o and transformation enthalpy change ΔH. T_o is defined as $T_o = 1/2(T_M + T_A)$, where T_M and T_A are the peak temperatures of the forward and the reverse transformations, and ΔH is obtained from the forward transformation. It is seen that the transformation temperatures of Fe0, Fe3 and Fe4 increased practically linearly with increasing the e/a ratio of the alloys. This observation is consistent with the findings of the effect of e/a ratio on transformation temperatures in Ni-Mn-Z (Z = Al, Ga, In, Sn and Sb) alloys[21-23]. It is also evident that the ΔH increased with increasing e/a ratio of the matrix.

Extending ΔH curve to zero tentatively defines the threshold value of e/a ratio below which the martensitic transformation is expected to vanish. The threshold value, as indicated by the arrow in Figure 3, is estimated to be e/a = 7.948. The e/a ratio value is larger than that of Fe5 alloy (e/a = 7.936 in Table 1), which explains the disappearance of martensitic transformation in Fe5 and Fe6 alloys.

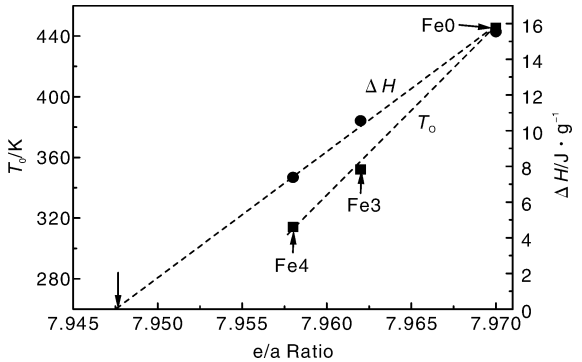

Fig. 3 Effects of Fe addition on transformation temperature $T_o = (T_M + T_A)/2$ and transformation enthalpy change ΔH. The arrow pointing to the e/a ratio axis indicates the threshold e/a ratio value below which the martensitic transformation is expected to vanish

3.3 Crystal structure

Figure 4 shows the crystal structures of the $Ni_{50}Mn_{38-x}In_{12}Fe_x$ alloys examined by X-ray diffraction at room temperature. The diffraction peaks can be indexed to be a non-modulated orthorhombic martensite structure in Fe0, Fe3 and Fe4 alloys. The observation of martensitic phase is consistent with the results obtained from DSC (Figure 2), which indicate the martensitic state at room temperature of these alloys. Fe4 and Fe5 alloys show a mixed structure of the bcc austenite and fcc γ phase based on the characteristic diffraction peaks in the spectra, which shows good agreement with the microstructure

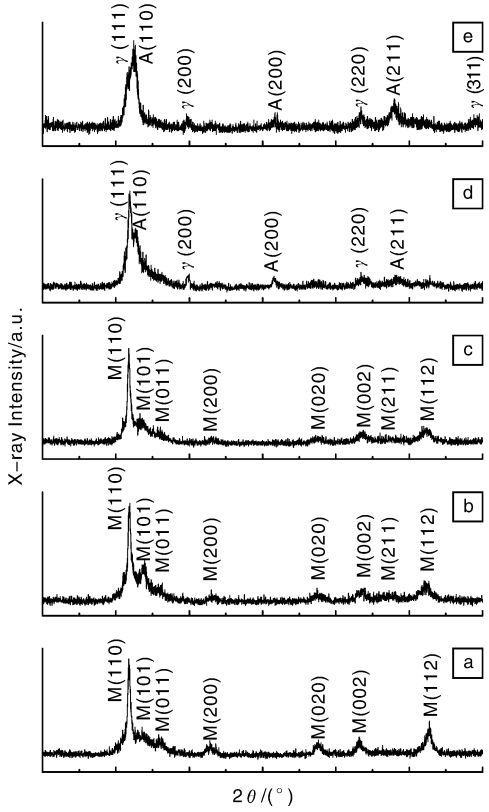

Fig. 4　X-ray spectra of the crystal structure of the $Ni_{50}Mn_{38-x}In_{12}Fe_x$ alloys at room temperature: (a) Fe0, (b) Fe3, (c) Fe4, (d) Fe5 and (e) Fe6 alloys

observation (Figure1 d, and e). Fe4 alloys shows γ phase particles in the matrix from the microstructure (Figure 1c), however such observation was absent based on the X-ray spectrum. It may be because that the amount of γ phase in the matrix was too little to be detected by the X-ray diffractometer employed in the study. The lattice parameters of the γ phase in Fe4, Fe5 and Fe6 are very close, with an average value of $a = 0.366$ nm at room temperature. The lattice parameter of the bcc austenite is determined to be $a = 0.299\ 5$ nm for Fe5 and Fe6 alloys. The lattice parameter of the orthorhombic martensite is determined to be $a = 0.321\ 7$ nm, $b = 0.295\ 6$ nm, $c = 0.285\ 1$ nm for Fe0, Fe3 and Fe4 alloys.

Figure 5 shows TEM observation of the microstructure and crystal structure of Fe5 and Fe6 alloys at room temperature. Micrograph a shows a bright field image of Fe5. Two phases are present in the microstructure, which are the matrix phase in dark contrast and the γ phase in light contrast. Selected area diffraction pattern (SADP) from area A of the matrix phase is shown in micrograph b, which can be indexed to B2 structure along its [001] zone axis. Presence of (010) reflection is the evidence of the superlattice B2 structure. Micrograph c shows the SADP of area B of the γ phase. The pattern is indexed to fcc system along [011] zone axis. Fe6 also exhibits two phases in the microstructure, including the matrix and the γ phases. The SADPs obtained from area C and D are presented in Micrograph e and f, respectively. Similarly, the matrix phase shows a B2 structure austenite and the γ phase is confirmed to be fcc structure.

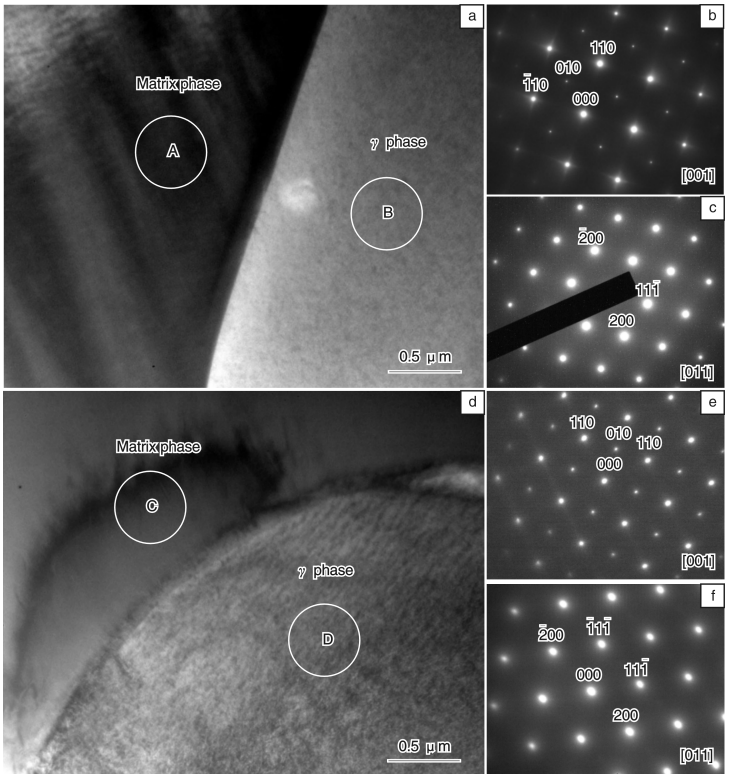

Fig. 5　Room temperature TEM micrographs and selected area diffraction patterns (SADPs) of the matrix and γ phase of Fe5 and Fe6 alloys: (a) bright field image of Fe5, (b) and (c) SADPs obtained from areas A and B of Fe5, (d) bright field image of Fe6, (e) and (f) SADPs obtained from areas C and D of Fe6

3.4 Magnetic properties

Figure 6 shows the zero-field cooling and field-cooling $M(T)$ curves of the $Ni_{50}Mn_{38-x}In_{12}Fe_x$ alloys in a small magnetic field of 3 979 A/m. The sample was first cooled down from 390 to 10 K inside the instrument without applying a magnetic field. A 3 979 A/m field was applied at 10 K and then the magnetization of the sample was measured upon heating to 390 K (Zero Field Cooling, ZFC). Subsequently, without removing the external field, the measurement was made upon cooling to 10 K (Field Cooling, FC).

As seen in Figure 6a, Fe0 presents a very small magnetization at 10 K when the 3 979 A/m field was applied, at 0.05 $A \cdot m^2 \cdot g^{-1} \times 10^{-3}$. The ZFC curve showed a broad hump at ~70 K. Passing the hump the magnetization started decreasing which was attributed to the Curie transition of the martensite, denoted as $T_C^M = 75$ K. Upon further heating along ZFC curve, another abrupt decrease of magnetization occurred at ~300 K, which is attributed to the Curie transition of the austenite. Though it was supposed to be the martensitic state at 300 K based on the DSC results (Figure 2), small amount of residual austenite may still exist at low temperatures in the matrix[22]. Thus, this temperature is denoted as T_C^A. The FC curve did not follow the route of the FC curve at below T_C^A, apparently due to the application of the magnetic field on this second cooling.

As seen in Figure 6b, the thermomagnetization behaviour of Fe3 is similar to that of Fe0. The Curie transition at ~315 K corresponds to that of the remnant austenite in this alloy. The Curie transition of the martensite is determined to be $T_C^M = 100$ K. Based on Figure 6c, the T_C^M and T_C^A are determined to be about 155 K and 315 K for Fe4 alloy, respectively. Fe5 and Fe6 showed different magnetization behaviour to the previous three samples. The magnetization was fairly constant at below or above T_C^A. These two samples showed no martensitic transformation within the testing temperature range, thus the absence of the Curie transition of the martensite. The T_C^A was determined to be 318 K for Fe5 and 321 K for Fe6 respectively.

It is seen that the T_C^A temperature increased from 300 K to 320 K with the increase of Fe addition from 0 to 6% (x). In the meantime, the T_C^M temperature was more significantly affected by Fe addition, increasing from 75 K to 155 K with increasing Fe addition up to 4% (x). The increase of the T_C^M and T_C^A indicate that Fe addition in the matrix enhances the magnetic ordering for both the austenitic and martensitic phases of the alloys. The enhancement of magnetic ordering is more pronounced in the martensite structure relative to the austenite structure.

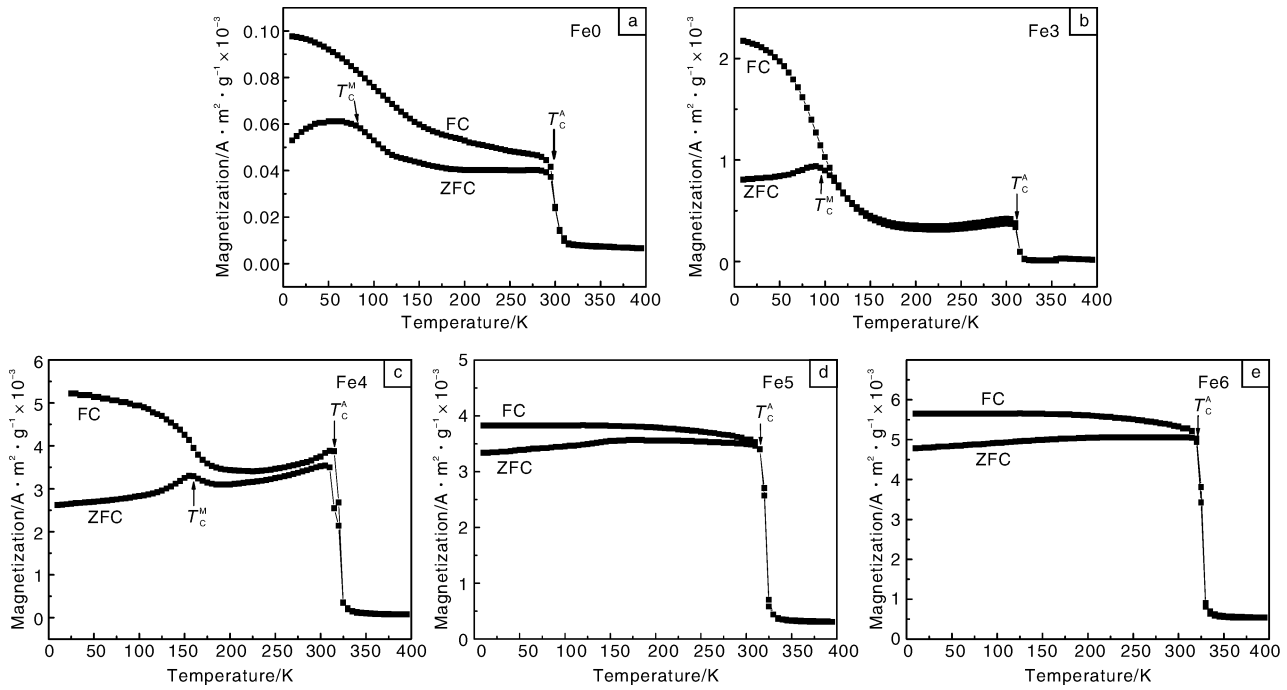

Fig. 6 ZFC and FC $M(T)$ curves of $Ni_{50}Mn_{38-x}In_{12}Fe_x$ alloys in a field of 3 979 A/m

Figure 7 shows the $M(H)$ curves of the $Ni_{50}Mn_{38-x}In_{12}Fe_x$ alloys at 5 K. The matrix phase is in martensitic state for Fe0, Fe3 and Fe4, whereas it is in austenitic state for Fe5 and Fe6 at 5 K. It is seen that Fe5 and Fe6 showed typical soft ferromagnetic behaviour, with saturation magnetization of 105 and 108 $A \cdot m^2 \cdot g^{-1} \times 10^{-3}$, respectively. The $M(H)$ data of Fe4 also showed the characteristics of ferromagnetic ordering in its martensitic state, but with a much reduced magnetization of 47 $A \cdot m^2 \cdot g^{-1} \times 10^{-3}$. The less steep initial slope of $M(H)$ curve of Fe3 indicates that some antiferromagnetic exchange may exist together with the short range ferromagnetic correlations in the martensitic phase. The coexistence of the ferromagnetic and antiferromagnetic structures can also be evidenced as the splitting between the ZFC and FC $M(T)$ curves (Figure 6b)[21-22]. The magnetization of Fe0 showed nearly linear dependence on the applied magnetic field up to 40 $A \cdot m^{-1} \times 7.958 \times 10^4$. The linearity of $M(H)$ data suggests that the antiferromagnetic structure may dominate in the magnetic state of the martensite. The saturation magnetizations are determined to be 13.6 and

27.7 A · m^2 · g^{-1} × 10^{-3} for Fe0 and Fe3, respectively.

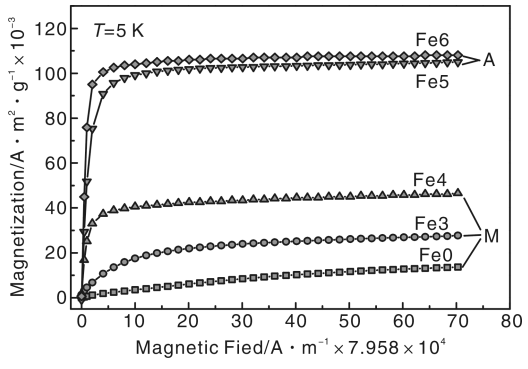

Fig. 7　Magnetization measurements of the $Ni_{50}Mn_{38-x}In_{12}Fe_x$ alloys at 5 K. A represents austenitic state and M represents martensitic state

In $Ni_{50}Mn_{38-x}In_{12}Fe_x$ alloys, extra Mn atoms occupy In sites, forming a ferromagnetic coupling between the Mn(Mn site) and Mn(In site) atoms in the austenitic phase[24]. Through the martensitic transformation, the distance between the Mn(Mn site)-Mn(In site) decreases and favours antiferromagnetic interaction in the martensitic phase. However, the Mn atoms at the Mn site still form ferromagnetic interaction in the martensitic phase. Therefore, the inhomogeneous magnetic structure is common to observe in the martensitic state of the Mn-rich Ni-Mn-Z(Z = In, Sn, Sb) alloys[21-22]. The magnetisation of Fe0 showed nearly linear dependence on the applied magnetic field up to 40 A · m^{-1} × 7.958 × 10^4. The linearity of $M(H)$ data suggests that it is antiferromagnetic in the martensitic state of this alloy.

4　Conclusions

This study investigated the effects of Fe substitution for Mn on the properties of Ni-Mn-In alloys. The main findings may be summarised as following:

(1) Fe substitution for Mn in $Ni_{50}Mn_{38-x}In_{12}Fe_x$ alloys at above 3% (x) causes formation of an fcc γ phase. The γ phase is a Ni-Mn-Fe solid solution phase with small amount of In dissolved. Formation of γ phase results in the decrease of Mn and increase of In contents of the matrix phase. Consequently, the e/a ratio of the matrix phase decreases with increasing Fe addition.

(2) The critical temperature (T_o), the enthalpy change (ΔH) of the martensitic transformation decreased with increasing Fe addition, due to the decrease of e/a ratio of the matrix phase caused by the formation of the γ phase. A threshold value of e/a ratio is identified at $\Delta H = 0$ to be 7.948, below which no martensitic transformation is expected in $Ni_{50}Mn_{38-x}In_{12}Fe_x$ alloys.

(3) The Curie temperature of the martensite (T_C^M) increased rapidly from 75 to 155 K with Fe addition to 4% (x), and that of the austenite (T_C^A) increased from 300 K to 320 K with Fe addition to 6% (x), The austenite shows much stronger ferromagnetic characteristic relative to that of the martensite. The ferromagnetic ordering of the martensite was enhanced with increasing Fe addition, due to the reduced content of antiferromagnetically coupled Mn in the alloys.

References

[1] Sutou Y, Imano Y, Koeda N, *et al.* Magnetic and Martensitic Transformations of NiMnX(X = In, Sn, Sb) Ferromagnetic Shape Memory Alloys [J]. *Appl Phys Lett*, 2004, 85 (19): 4 358 - 4 360.

[2] Kainuma R, Imano Y, Ito W, *et al.* Metamagnetic Shape Memory Effect in a Heusler-Type $Ni_{43}Co_7Mn_{39}Sn_{11}$ Polycrystalline Alloy [J]. *Appl Phys Lett*, 2006, 88: 192513 - 1 - 3.

[3] Kainuma R, Imano Y, Ito W, *et al.* Magnetic-Field-Inudced Shape Recovery by Reverse Phase Transformation [J]. *Nature*, 2006, 439: 957 - 960.

[4] Kainuma R, Ito W, Umetsu R Y, *et al.* Magnetic Field-Induced Reverse Transformation in B2-Type NiCoMnAl Shape Memory Alloys [J]. *Appl Phys Lett*, 2008, 93 (9): 091 906 - 1 - 3.

[5] Yu S Y, Cao Z X, Ma L, *et al.* Realization of Magnetic Field-Induced Reversible Martensitic Transformation in NiCoMnGa Alloys [J]. *Appl Phys Lett*, 2007, 91 (10): 102 507 - 1 - 3.

[6] Yu S Y, Ma L, Liu G D, *et al.* Magnetic Field-Induced Martensitic Transformation and Large Magnetoresistance in NiCoMnSb Alloys [J]. *Appl Phys Lett*, 2007, 90 (24): 242 501 - 1 - 3.

[7] Wu Z, Liu Z, Yang H, *et al.* Metamagnetic Phase Transformation in Mn50Ni37In10Co3 Polycrystalline Alloy [J]. *Appl Phys Lett*, 2011, 98 (6): 061 904 - 1 - 3.

[8] Ito W, Imano Y, Kainuma R, *et al.* Martensitic and Magnetic Transformation Behaviors in Heusler-Type NiMnIn and NiCoMnIn Metamagnetic Shape Memory Alloys [J]. *Metall Mater Trans A*, 2007, 38 (4): 759 - 766.

[9] Masdeu F, Pons J, Santamarta R, *et al.* Effect of Precipitates on the Stress-Strain Behavior under Compression in Polycrystalline Ni-Fe-Ga Alloys [J]. *Materials Science and Engineering: A*, 2008, 481 - 482: 101 - 104.

[10] Liu J, Xie H, Huo Y, *et al.* Microstructure Evolution in CoNiGa Shape Memory Alloys [J]. *J Alloys Compd*, 2006, 420 (1 - 2): 145 - 157.

[11] Tanaka Y, Oikawa K, Sutou Y, *et al.* Martensitic Transition and Superelasticity of Co-Ni-Al Ferromagnetic Shape Memory Alloys with β-γ Two-Phase Structure [J]. *Materials Science and Engineering: A*, 2006, 438 - 440: 1 054 - 1 060.

[12] Yang S, Ma Y, Jiang H, *et al.* Microstructure and Shape-Memory Characteristics of $Ni_{56}Mn_{25-x}Co_xGa_{19}$ (x = 4, 8) High-Temperature Shape-Memory Alloys [J]. *Intermetallics*, 2011, 19 (2): 225 - 228.

[13] Ma Y, Yang S, Liu Y, *et al.* The Ductility and Shape-Memory Properties of Ni-Mn-Co-Ga High-Temperature Shape-Memory Alloys [J]. *Acta Mater*, 2009, 57 (11): 3 232 - 3 241.

[14] Xin Y, Li Y, Chai L, *et al.* Shape Memory Characteristics of Dual-Phase Ni-Mn-Ga Based High Temperature Shape Memory Alloys [J]. *Scripta Mater*, 2007, 57 (7): 599 - 601.

[15] Wang H B, Sui J H, Liu C, *et al.* Martensitic Transformation and Shape Memory Effect in Ni54.75Mn13.25Fe7Ga25 Ferromagnetic Shape Memory Alloy [J]. *Materials Science and Engineering: A*, 2008, 480 (1 - 2): 472 - 476.

[16] Feng Y, Sui J, Gao Z, *et al.* Investigation on Martensitic Transformation and Mechanical Properties of the $Ni_{50}Mn_{37-x}Sn_{13}Fe_x$ (x = 0, 2, 5, 10) Alloys [J]. *Int J Mod Phys B*, 2010, 23: 1 803 - 1 808.

[17] Feng Y, Sui J H, Gao Z Y, *et al.* Investigation on Martensitic Transformation Behavior, Microstructures and Mechanical Properties of Fe-Doped Ni-Mn-In Alloys [J]. *Mater Sci Eng A*, 2009, 507 (1 - 2): 174 - 178.

[18] Passamani E C, Xavier F, Favre-Nicolin E, *et al.* Magnetic Properties of NiMn-Based Heusler Alloys Influenced by Fe Atoms Replacing Mn [J]. *J Appl Phys*, 2009, 105 (3): 033 919 - 033 926.

[19] Fukushima K, Sano K, Kanomata T, *et al.* Phase Diagram of Fe-Substituted Ni-Mn-Sn Shape Memory Alloys [J]. *Scripta Mater*,

2009, 61 (8): 813 - 816.
[20] Wu Z, Liu Z, Yang H, *et al*. Metallurgical Origin of the Effect of Fe Doping on the Martensitic and Magnetic Transformation Behaviours of $Ni_{50}Mn_{40-x}Sn_{10}Fe_x$ Magnetic Shape Memory Alloys [J]. *Intermetallics*, 2011, 19 (4): 445 - 452.
[21] Krenke T, Acet M, F Wassermann E, *et al*. Martensitic Transitions and the Nature of Ferromagnetism in the Austenitic and Martensitic States of Ni-Mn-Sn Alloys [J]. *Physical Review B*, 2005, 72 (1): 014 412 - 1 - 9.
[22] Krenke T, Acet M, F Wassermann E, *et al*. Ferromagnetism in the Austenitic and Martensitic States of Ni-Mn-In Alloys [J]. *Physical Review B*, 2006, 73 (17): 174 413 - 1 - 10.
[23] Krenke T, Moya X, Aksoy S, *et al*. Electronic Aspects of the Martensitic Transition in Ni-Mn Based Heusler Alloys [J]. *J Magn Magn Mater*, 2007, 310 (2, Part 3): 2 788 - 2 789.
[24] Kanomata T, Yasuda T, Sasaki S, *et al*. Magnetic Properties on Shape Memory Alloys $Ni_2Mn_{1+x}In_{1-x}$ [J]. *J Magn Magn Mater*, 2009, 321: 773 - 776.